ACS APPLIED MATERIALS & INTERFACES

Research Article

www.acsami.org

Graphene as an Efficient Interfacial Layer for Electrochromic Devices

Feng Lin,[†,‡,§] Justin B. Bult,[†,§] Sanjini Nanayakkara,[†] Anne C. Dillon,[†] Ryan M. Richards,[‡] Jeffrey L. Blackburn,*[,†] and Chaiwat Engtrakul*[,†]

[†]National Renewable Energy Laboratory, Golden, Colorado 80401, United States

[‡]Department of Chemistry and Geochemistry & Materials Science Program, Colorado School of Mines, Golden, Colorado 80401, United States

Supporting Information

ABSTRACT: This study presents an interfacial modification strategy to improve the performance of electrochromic films that were fabricated by a magnetron sputtering technique. High-quality graphene sheets, synthesized by chemical vapor deposition, were used to modify fluorine-doped tin oxide substrates, followed by the deposition of high-performance nanocomposite nickel oxide electrochromic films. Electrochromic cycling results revealed that a near-complete monolayer graphene interfacial layer improves the electrochromic performance in terms of switching kinetics, activation period, coloration efficiency, and bleached-state transparency, while maintaining ~100% charge reversibility. The present study offers an alternative route for improving the interfacial properties between electrochromic and transparent conducting oxide films without relying on conventional methods such as nanostructuring or thin film composition control.

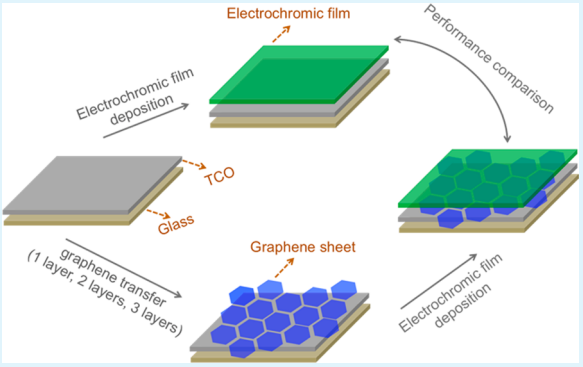

KEYWORDS: *graphene, nickel oxide, electrochromic, interface, lithium intercalation*

INTRODUCTION

Interface engineering is an intensive research thrust for various renewable energy technologies, including electrochromics,[1,2] photovoltaics,[3,4] and lithium batteries.[5] One purpose of interface engineering within these technologies is to ease migration of electrons, ions, or both across interfaces, enabling fast charge transfer. Electrochromic (EC) devices are typically multilayered structures with several interfaces that dictate the ultimate device performance metrics, such as the kinetics of switching between the bleached (high transmittance) and colored (low transmittance) states.[6,7] Previous studies have demonstrated that the electronic properties of the interface between the transparent conductive oxide (TCO) and electrochromic film can establish charge transfer impedance that is detrimental to the switching kinetics of electrochromic devices and prevents the devices from attaining the fully bleached or colored state.[1] Typically, devices must be cycled, often for hundreds of cycles, to reduce this charge transfer impedance and obtain the fully bleached state needed for deployment in the field.[8] This so-called "activation period" increases the ultimate cost of an electrochromic window, since manufacturers must perform this cycling routine before releasing windows to consumers.

Recently, Ostermann et al. reported that a thin Au layer between a TCO and wet-chemical synthesized WO_3 thin film is beneficial for switching kinetics.[1] The authors attributed the improved switching kinetics to the increased electrical conductivity of the Au-coated TCO substrate compared to the pristine TCO substrate. However, the Au coating tends to reduce the transparency of the bleached state due to the surface plasmon resonance, even with an ultrathin coating.[9,10] Furthermore, it is still unknown whether this kind of interfacial modification influences the activation period for EC devices. Finally, the usage of Au handicaps the cost-effective fabrication of EC devices thereby inhibiting large-scale manufacturing. Thus, new interfacial modification strategies are needed for high-performance EC devices that are based on cost-effective materials with simultaneously high transparency and conductivity.

Recently, graphene thin films have been integrated into a number of optoelectronic devices, including photovoltaics,[11−13] batteries,[14−16] and electrochromic windows.[17−19] Whereas all of these technologies benefit from the very high lateral conductivity of the graphene sheet, applications like photovoltaics and electrochromics also benefit from the high optical transparency of single/multilayer graphene films.[20,21] In all of these emerging applications, interfacial charge transfer between graphene and the device active material plays a critical role in facilitating high-performance devices. We were motivated by the experimentally demonstrated high charge mobilities and

Received: February 26, 2015
Accepted: May 7, 2015
Published: May 7, 2015

DOI: 10.1021/acsami.5b01777
ACS Appl. Mater. Interfaces 2015, 7, 11330−11336

high transparency of large-area graphene sheets grown by chemical vapor deposition (CVD)[22−24] to explore the potential enhancement of interfacial charge transfer between the nickel oxide (NiO) counter electrode layer and TCO in a typical electrochromic device structure.

Herein, we employ single- to multilayer graphene films, produced by CVD and transferred via a heat transfer tape method,[22] for interfacial modification of high-performance nanocomposite NiO electrochromic films.[25] Graphene layers are shown to reduce both the switching time and activation period, with the optimum performance found for two sequentially transferred graphene layers. Raman microscopy demonstrates that the transfer of CVD-grown graphene to the fluorine-doped tin oxide (FTO) substrate is incomplete, in contrast to relatively complete transfers that are readily obtained for transfers to Si/SiO_x substrates. Two sequential graphene transfers produce near-complete coverage of the FTO, whereas additional transfers produce multilayers, which helps explain the optimal performance of EC electrodes modified with two layers. The high optical transparency and presumably low charge transfer impedance of the graphene interfacial layers enable the realization of a > 95% transmissive bleached state (at λ = 670 nm, T_{670}) within 100 cycles, a dramatic improvement over the device with no modification (T_{670} < 90% after 500 cycles). Thus, the present study demonstrates an economically viable solution for interface engineering in electrochromic devices and provides an attractive alternative for next generation thin film electrochemical energy storage devices.

EXPERIMENTAL METHODS

Synthesis and Transfer of Graphene. The experimental procedure for preparing electrochromic active electrodes is shown in Scheme 1. The single-layer-graphene (SLG) was grown via copper (Alpha Aesar 13382) supported chemical vapor deposition (CVD).[22−24] The growth was performed under low-pressure (100 mTorr) using a 2-in. bore hot-wall CVD reactor operating at 1000 °C. Flow conditions were 35 standard cubic centimeters per minute (sccm) of methane and 7 sccm of hydrogen for 30 min at growth temperature. The copper substrate (1.5 × 2 in.) was placed in the center of the furnace supported by a fused quartz plate in a sealed quartz tube reaction chamber. Following graphene growth, the reactor was allowed to cool at 10 °C/min under the same hydrogen−methane conditions. Upon completion of the growth process, heat transfer tape (HTT, Revalpha 3195M) was applied to the graphene on copper, using static pressure of 50 psi held for 1 min. The HTT−graphene−copper laminate was then placed within an etchant bath of 0.1 M ammonium persulfate to remove the copper growth substrate. After 24 h, the HTT-graphene sheet was removed and washed in deionized water to remove any residual etchant and allowed to dry in air for 30 min before application to either Si/SiO_x or the FTO-coated glass substrates (Hartford Glass CO, Inc. TEC 15, 1.5 in. × 0.82 in. × 2.3 mm) used for preparing EC samples. Before graphene transfer to FTO, the FTO substrates were cleaned successively with soapy water, deionized water, acetone, isopropanol, and dried under flowing N_2. Application of the HTT−graphene laminate to the FTO substrate was carried out using low-pressure hand rolling. The HTT-graphene was carefully placed on the FTO substrate and hand-pressed until all observable discontinuities (air bubbles, low-adhesion sections) were eliminated. The FTO-graphene-HTT material was then placed on a hot plate at 120 °C, thereby delaminating the HTT from the graphene and FTO. This process leaves the graphene adhered to the FTO. The transfer process was performed in an Ar-filled glovebox.

Scheme 1. Schematic Illustration of the Preparation for Electrochromic Electrodes with and without a Graphene Interface Layer[a]

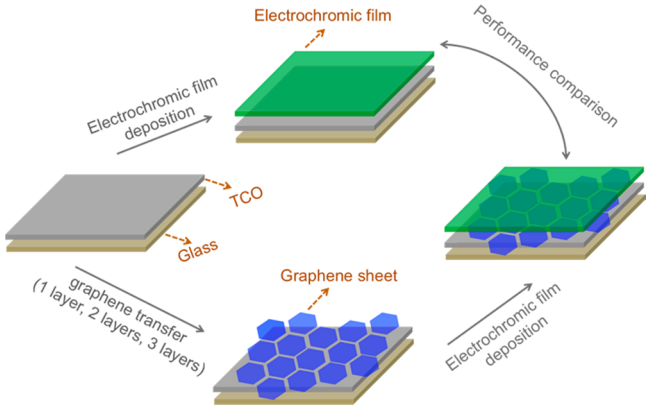

[a]Corresponding layer information is labeled in the scheme.

Deposition of Electrochromic Films. The procedure for the deposition of electrochromic films has been described in detail previously.[25−27] Radio frequency (RF) magnetron sputtering was preformed on an Angstrom EvoVac deposition system housed in a glovebox under an argon atmosphere. A 3 in. diameter metal alloy target, Ni−Zr (80−20 at. %), was purchased from ACI Alloys, while a 3 in. diameter ceramic Li_2O target (99.9%) supported on a molybdenum backing plate was purchased from Plasmaterials, Inc. The gun powers for the metal alloy targets and ceramic target were 60 and 45 W, respectively. These gun powers resulted in optimal performing electrochromic films with a chemical formula of $Li_{2.34}NiZr_{0.28}O_x$. Chemical composition of the electrochromic films was determined from inductively coupled plasma mass spectrometry (ICP-MS). The target-substrate distance was 10 cm and remained constant throughout the study, and no additional heating was applied to the substrates (i.e., pristine and graphene-coated FTO substrates). The base pressure and total deposition pressure were 10^{-7} Torr and 2 mTorr, respectively. The Ar/O_2 gas mixture ratio was fixed at 1/2 throughout the study. The film thickness was confirmed by a Veeco Dektak 8 Profilometer and was ∼200 nm for all the studied EC films.

Materials Characterization. Raman mapping was performed on a Witec Alpha 300 system with a 532 nm laser utilizing a 100× objective. Three peaks were tracked for map creation: the disorder generated D peak at $\omega \approx 1350$ cm^{-1}, the single resonance G peak at $\omega \approx 1585$ cm^{-1}, and the double resonance-two phonon G′ (or 2D) peak at $\omega \approx 2700$ cm^{-1}.[28,29] The structure of the as-deposited nickel oxide nanocomposite electrochromic films was studied elsewhere[25] and is not presented in this paper. Briefly, the electrochromic films are composed of nickel oxide crystallites imbedded into an amorphous oxide matrix.[25]

Performance Evaluation. Performance evaluation was performed according to a standard protocol.[25,26] In detail, electrochromic properties were measured in a liquid electrolyte half-cell where the electrolyte was 1 M lithium perchlorate ($LiClO_4$) dissolved in propylene carbonate (PC). Cyclic voltammetry (CV) was carried out using a BioLogic VMP3 multichannel potentiostat with a scan rate of 20 mV/s and a voltage range of 1.7−4.2 V vs Li/Li^+. In situ transmittance was measured using a diode laser at 670 nm (T_{670}). Switching kinetics (i.e., coloration and bleaching kinetics) were measured under potential step cycling from 1.7 to 4.2 V vs Li/Li^+, where each potential step was maintained for 2 min. The switching speed is defined as the time required to achieve ∼90% of total transmittance change within a potential step. The switching kinetics were measured for two different sets of samples: (1) as-deposited, fresh samples and (2) activated samples (i.e., samples far beyond the electrode activation period). All electrochemical measurements were carried out under an argon atmosphere in a glovebox. The samples were transferred from the sputtering chamber to testing cells without exposure to air or moisture.

DOI: 10.1021/acsami.5b01777
ACS Appl. Mater. Interfaces 2015, 7, 11330−11336

RESULTS AND DISCUSSION

Raman spectroscopy and spatial mapping was used to characterize the quality and coverage of the transferred graphene sheets, as shown in Figures 1 and 2. Three Raman peaks were tracked for all samples: the disorder generated D peak at $\omega \approx 1350$ cm^{-1}, the single resonance G peak at $\omega \approx 1585$ cm^{-1}, and the double resonance-two phonon G′ peak at $\omega \approx 2700$ cm^{-1}. For each peak, we used Raman mapping to track the intensity, full width at half-maximum (fwhm), and center position as a function of spatial position. The full-width at half-maximum (fwhm) of the G′ peak, as well as the G′/G intensity ratio can be used as indicators for the number of sp^2 graphene layers.[28] Additionally, the defect-activated D peak can be used as an indicator of the spatial distribution of defects and grain boundaries for the transferred graphene.

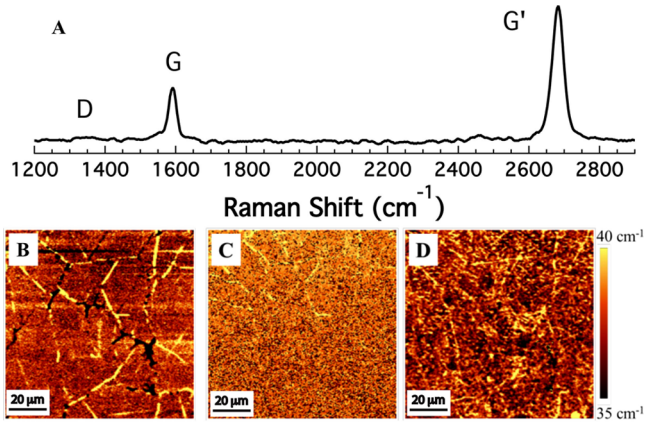

Figure 1. (A) Micro-Raman spectrum of monolayer graphene transferred to Si/100 nm SiO_x wafer. (B) G′ peak (≈2700 cm^{-1}) intensity map showing graphene domain structure and continuous nature of graphene when transferred to the smooth Si/SiO_x surface. (C) D peak (≈1350 cm^{-1}) intensity showing domain boundary intensity and little to no observable D peak within the graphene domain. (D) G′ peak fwhm showing no observable multilayer sections (fwhm of multilayers > ∼ 40 cm^{-1}) in this map.

Figure 1 shows the Raman spectrum and several Raman maps for a single transfer (1L) of our CVD-grown graphene to a Si/SiO_x wafer. The narrow single-Lorentzian fwhm value of ∼33 cm^{-1} for the G′ peak[28,29] and the G′/G intensity ratio of ∼2.5 indicates that our CVD growth produces high-quality monolayer graphene, whereas the spatial uniformity of the G′ map in Figure 1b demonstrates that the transferred graphene is predominantly a continuous monolayer when transferred to a smooth surface such as a silicon wafer. Some very small tears in the graphene sheet are visible as black spots in Figure 1b. The D peak (≈1350 cm^{-1} (Figure 1c)) intensity delineates the graphene domain boundaries, and there is little to no observable D peak within the graphene domain, indicating high-quality graphene.[30,31] The G′ peak fwhm (Figure 1d) shows no observable multilayer sections in this map (e.g., > 40 cm^{-1} fwhm, requiring multiple Lorentzians), whereas limited multilayer nucleation centers can be observed elsewhere.

Figure 2a–c shows AFM topography images of unmodified FTO and FTO modified with 1L graphene. Comparison of the 0L-FTO and 1L-FTO images clearly demonstrates the successful transfer of graphene. A variety of small and large grains of graphene can be seen in the 1L-FTO samples, although the coverage of graphene appears to be significantly more heterogeneous and incomplete compared to the 1L graphene sample on Si/SiO_x.

Raman maps for two sequential transfers (1L and 2L) of graphene to the FTO substrates (Figures 2d–i) support the

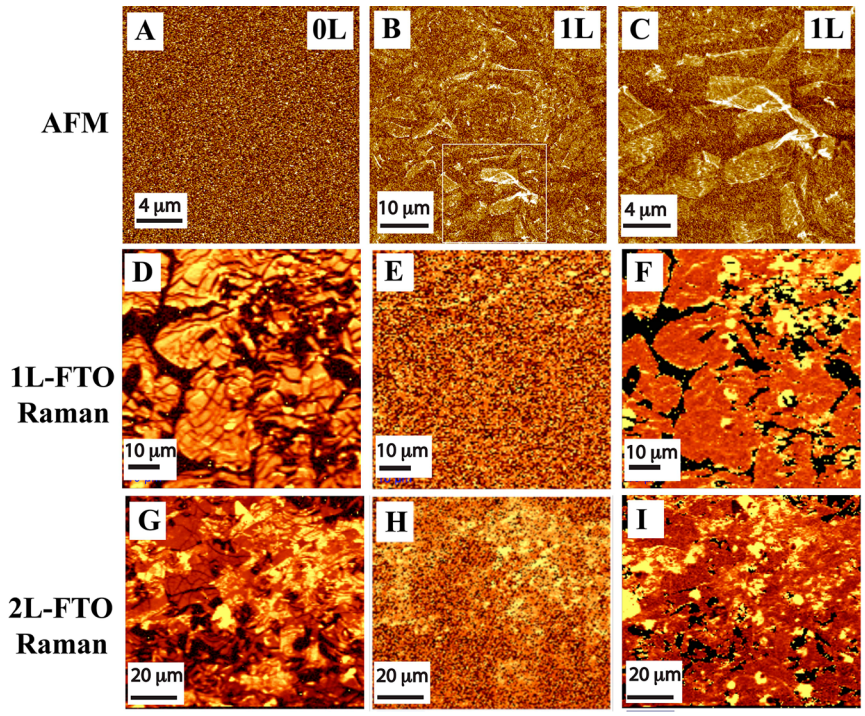

Figure 2. AFM topography images of (A) unmodified FTO, 0L, and (B and C) 1L graphene on FTO. Raman maps of (D–F) 1L graphene and (G–I) 2L graphene transferred to FTO substrate using HTT method. (D and G) G′ peak (≈2700 cm^{-1}) intensity map. (E and H) D peak (≈1350 cm^{-1}) intensity map. (F and I) G′ peak fwhm map. Peak fwhm (yellow color) in panel F is 45 cm^{-1} and peak fwhm in panel I is 50 cm^{-1}.

DOI: 10.1021/acsami.5b01777
ACS Appl. Mater. Interfaces 2015, 7, 11330–11336

heterogeneous graphene coverage observed by AFM on FTO. It is apparent from the Raman maps that the graphene layer is only partially transferred and is torn to some degree when transferred to FTO. Many bare spots of FTO can be seen as large black areas in the G′ intensity (Figure 2d) and fwhm (Figure 2f) maps for the 1L transfer. The partial transfer, as well as the observable tearing of the graphene, is likely due to the roughness and low adhesion of the FTO substrate, which makes it necessary to use higher pressure during the pressing procedure. However, the graphene that has been transferred is of high quality based on the lack of a significant D peak (Figure 2e) and the limited two layer nucleating centers (Figure 2f). Increasing the number of graphene transfers (2L-FTO) results in better graphene coverage and a greater degree of second and third layer sections (Figure 2g–i). The maps of the 2L graphene-coated FTO contains very few bare areas, and the G′ fwhm map indicates that the majority of the graphene film is monolayer, with many small areas being bilayer.[28,29] Beyond two transfers, the graphene thin film becomes predominantly multilayer (not shown).

For electrochromic studies, state-of-the-art nanocomposite nickel oxide electrochromic films ($Li_{2.34}NiZr_{0.28}O_x$)[25] were deposited onto either FTO or graphene-coated FTO substrates. All electrochromic films were fabricated in the same period of time to eliminate possible systematic errors, and the $Li_{2.34}NiZr_{0.28}O_x$ film thickness remains constant for all the samples (~200 nm).

Electrochromic switching kinetics are presented in Figure 3. Switching kinetics (i.e., bleaching kinetics, coloration kinetics)

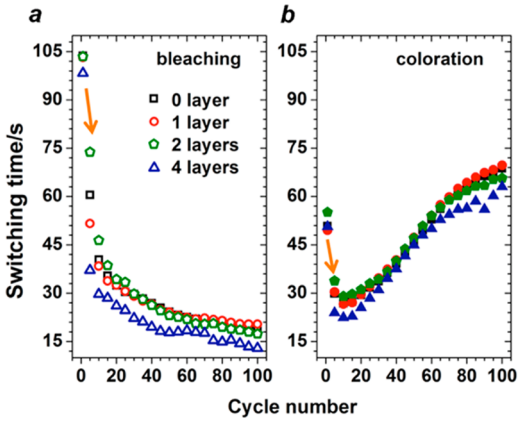

Figure 3. (a) Bleaching kinetics and (b) coloration kinetics of the resulting electrochromic films as a function of cycle number using CA technique. The black, red, green, and blue plots represent 0-layer, 1-layer, 2-layer, and 4-layer graphene interfacial layers, respectively. The arrows indicate a great improvement in switching kinetics after the first cycle. Cycling data obtained from as-deposited fresh samples.

are defined by the time required for 90% transmittance change upon a potential switching step. All studied electrodes show significantly improved switching kinetics in the second cycles compared to the corresponding first cycles (indicated by the arrows in Figure 3), which is most likely due to the improved electrolyte wetting on the thin film electrodes. In subsequent cycles, bleaching and coloration kinetics experience opposite trends with the increase of cycle number. The optimal coloration kinetics were observed at around the 10th cycle. Presumably, structural changes during electrochemical cycling impose opposite effects on bleaching and coloration processes. No significant difference in kinetics is observed for low numbers of graphene transfer (i.e., 0-layer, 1-layer, 2-layer) in the first ~60 cycles, whereas the electrode with 4 graphene interfacial layers consistently exhibits the fastest switching kinetics over this same time period. However, above ~60 cycles, the bleaching and coloration kinetics for the 2L graphene-modified electrode begin to improve at a faster rate relative to the kinetics of the 0L and 1L samples.

Appreciable activation periods for electrochromic films could increase their manufacturing cost because this activation period implies significant cycling by the manufacturer before transferring an electrochromic product to market. The activation period for the graphene-modified EC electrodes was assessed by recording T_{670} through electrochromic films under CV cycling. Similar to the bleaching kinetics shown in Figure 3a, in situ optical modulation exhibits an obvious optical activation period for the bleached-state transmittance (upper curves in Figure 4a). On the contrary, no activation period is observed

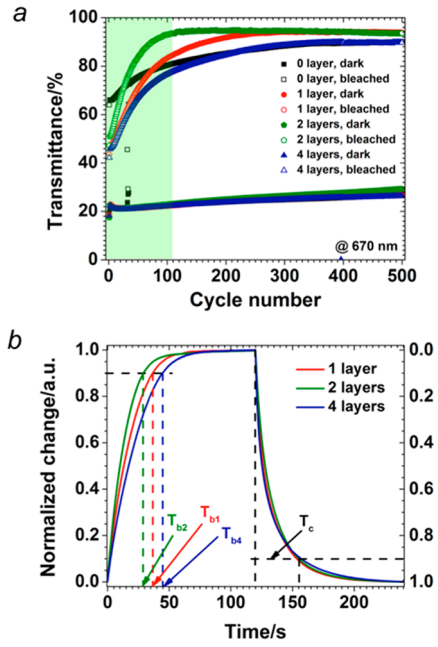

Figure 4. (a) In situ optical modulation (at 670 nm) during CV cycling with a scan rate of 20 mV/s, where the shadow region indicates the shortest activation period for the electrode with 2 layers of graphene sheets. The curves at the lower and upper portions represent dark and bleached states, respectively. (b) Switching kinetics of electrochromic films after 500 CV cycles (far beyond the electrode activation period).

for the dark state transmittance (lower curves in Figure 4a). The activation period of the bleached-state transmittance is attributed in part to the poorer bleaching kinetics in the early stage of electrochemical cycling (Figure 3a). For the standard device, prepared on FTO, this activation period is quite long and T_{670} is below 90% even after 500 cycles. In stark contrast, the device modified with 1 graphene transfer (1L) has already attained an improved $T_{670} \approx 95\%$ after 300 cycles, and the device modified with 2 graphene transfers (2L) reaches $T_{670} \approx 95\%$ after only 100 cycles. The significantly reduced activation period when the graphene interlayer was present indicates that the graphene interlayer may assist the electron transfer from FTO to electrochromic materials. It is noted that the dark state

DOI: 10.1021/acsami.5b01777
ACS Appl. Mater. Interfaces 2015, 7, 11330–11336

transmittance is independent of the number of graphene interfacial layers.

Previous studies show that the transmittance of a graphene-coated glass substrate is dependent on the number of graphene transfers, with each layer contributing to a relatively flat (spectrally) ~2.3% absorbance.[32] Thus, it was expected that the graphene-modified EC electrodes would have slightly lower transmittance than the standard device without graphene modification if all other properties of the electrochromic device (e.g., interfacial charge transfer impedance) are unaffected by the graphene interfacial layer. Importantly, after 500 cycles the bleached-state transparencies of thin film electrodes 1L and 2L graphene transfers are slightly better than that of the pristine electrode (i.e., no graphene; Figure 4a and Figure S1, SI). The in situ transmittance at 670 nm as a function of voltage is shown in Figure S2 (SI), which further demonstrates that 1L and 2L graphene transfers yielded slightly improved transparency at the 500th cycle. Bleached-state transparency is determined by the degree of electron intercalation and neutralization with hole states in the NiO_6 octahedral unit.[25] Therefore, our results demonstrate that graphene interfacial layers can facilitate the neutralization of hole states within the electrochromic active layer, an effect that most likely results from a decrease in the interfacial charge transfer impedance. However, when graphene coverage increases beyond two transfers, the activation period for the four-layer electrode becomes longer than the pristine electrode; meanwhile, no improvement for bleached-state transparency is observed. This result suggests that the improvements afforded by a near-complete monolayer of graphene (2L sample, as determined by Raman mapping) are not attained once the graphene interfacial layer consists largely of multiple layers (e.g., 4L sample). These diminishing returns may point to interfacial charge transfer in samples modified with multilayers being limited by the out-of-plane (sheet-to-sheet) conductivity of graphene, which is known to be significantly lower than the in-plane conductivity.

Switching kinetics after an activation period of 500 cycles for each device are shown in Figure 4b. The best bleaching kinetics are observed in the 2L graphene-modified electrode, while coloration kinetics show negligible dependence on the graphene interfacial layer. The data indicate that with prolonged cycling, the 2L graphene-modified EC electrode maintains the best switching kinetics and highest bleached state transmittance, enabling significantly higher performance EC electrodes relative to devices built on unmodified FTO.

Coloration efficiency (CE) is a critical metric and is measured as the change in optical density (ΔOD) per unit of charge density (ΔQ) extracted from electrochromic films. High CE indicates that one can achieve large optical contrast with small charge intercalation thus enabling more efficient switching process. As shown in Figure 5, the CE of electrodes with graphene interfacial layers was improved relative to the blank electrochromic film. Furthermore, all of the studied electrodes show extremely high charge reversibility (~100%) with extended cycle number (Figure 5).

Our current hypothesis regarding the mechanism underlying the improved performance of graphene-modified electrochromics invokes improved charge transfer from the TCO layer to the active layer. However, the rigorous quantification of the charge transfer metrics (e.g., interfacial charge transfer resistance and kinetics) across the multiple layers involved in the devices is challenging. Our initial conducting AFM results (Figure S3, SI), along with the well-characterized anisotropy of

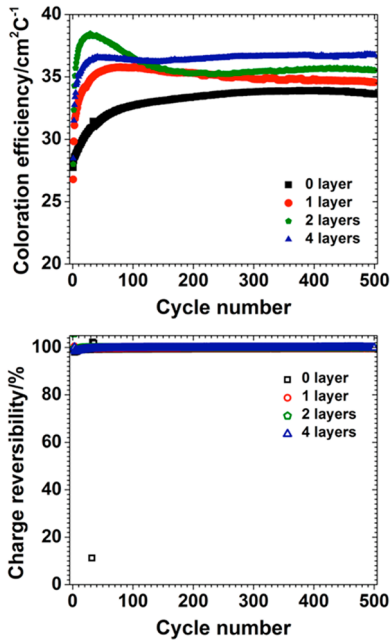

Figure 5. Dependence of coloration efficiency on the CV cycle number (top). Dependence of charge reversibility on the CV cycle number (bottom).

graphene's in-plane (*a* axis) and out-of-plane (*c* axis) conductivity[33,34] and spatially heterogeneous conductivity of typical TCOs,[35] suggest that the interfacial charge transfer between graphene and the $Li_{2.34}NiZr_{0.28}O_x$ active layer is likely a complex function of the spatially averaged charge transfer resistance and kinetics (from FTO to graphene, graphene to active layer, and between graphene sheets). Ideally, follow-on studies involving impedance spectroscopy and perhaps transient optical studies will help clarify these issues but are beyond the scope of this study.

CONCLUSION

Graphene was used as an optically transparent interfacial modifier layer between the TCO and state-of-the-art electrochromic films. Raman mapping spectroscopy shows successful transfer of high-quality graphene sheets onto the TCO, although each transfer is incomplete due presumably to the surface roughness of the TCO. Electrochromic evaluation demonstrates that a near-complete graphene monolayer, attained after two sequential graphene transfers, improves the electrochromic performance of a state-of-the-art NiO EC electrodes in terms of switching kinetics, activation period, coloration efficiency, and bleached-state transparency. These promising results encourage further detailed experiments to uncover the fundamental mechanisms underlying the enhancements observed in this study. Finally, we anticipate that similar graphene interfacial modification may benefit other electrochemical systems, such as thin film batteries.

ASSOCIATED CONTENT

Supporting Information

Full-spectrum UV–vis–NIR spectra and cyclic voltammetry and in situ transmittance curves of the electrochromic electrodes; conducting atomic force microscopy of the graphene interfaces. The Supporting Information is available

DOI: 10.1021/acsami.5b01777
ACS Appl. Mater. Interfaces 2015, 7, 11330–11336

free of charge on the ACS Publications website at DOI: 10.1021/acsami.5b01777.

AUTHOR INFORMATION

Corresponding Authors

*E-mail: jeffrey.blackburn@nrel.gov.

*E-mail: chaiwat.engtrakul@nrel.gov.

Present Address

(F.L.) Environmental Energy Technologies Division, Lawrence Berkeley National Laboratory, Berkeley, CA 94720, United States.

Author Contributions

§These authors contributed equally to this work.

Notes

The authors declare no competing financial interest.

ACKNOWLEDGMENTS

C.E., F.L., A.C.D., and R.M.R. were supported by the U.S. Department of Energy under contract number DE-AC36-08-GO28308 with the National Renewable Energy Laboratory as part of the DOE Office of Energy Efficiency and Renewable Energy Office of Building Technologies Program. J.L.B., J.B.B., and S.N. were funded by the NREL's Laboratory Discretionary Research and Development (LDRD) program.

REFERENCES

(1) Ostermann, R.; Smarsly, B. Does Mesoporosity Enhance Thin Film Properties? A Question of Electrode Material for Electrochromism of WO_3. *Nanoscale* **2009**, *1*, 266−270.

(2) Lin, F.; Nordlund, D.; Weng, T.-C.; Moore, R. G.; Gillaspie, D. T.; Jones, K. M.; Dillon, A. C.; Richards, R. M.; Engtrakul, C. Solid-State Conversion Reaction to Enhance Charge Transfer in Electrochromic Materials. *Adv. Mater. Interfaces* **2015**, *2* (6), 1400523.

(3) Worfolk, B. J.; Hauger, T. C.; Harris, K. D.; Rider, D. A.; Fordyce, J. A. M.; Beaupré, S.; Leclerc, M.; Buriak, J. M. Work Function Control of Interfacial Buffer Layers for Efficient and Air-Stable Inverted Low-Bandgap Organic Photovoltaics. *Adv. Energy Mater.* **2012**, *2*, 361−368.

(4) Steirer, K. X.; Ndione, P. F.; Widjonarko, N. E.; Lloyd, M. T.; Meyer, J.; Ratcliff, E. L.; Kahn, A.; Armstrong, N. R.; Curtis, C. J.; Ginley, D. S.; Berry, J. J.; Olson, D. C. Enhanced Efficiency in Plastic Solar Cells via Energy Matched Solution Processed NiO_x Interlayers. *Adv. Energy Mater.* **2011**, *1*, 813−820.

(5) Ohta, N.; Takada, K.; Zhang, L.; Ma, R.; Osada, M.; Sasaki, T. Enhancement of the High-Rate Capability of Solid-State Lithium Batteries by Nanoscale Interfacial Modification. *Adv. Mater.* **2006**, *18*, 2226−2229.

(6) Granqvist, C. G. Oxide-Based Chromogenic Coatings and Devices for Energy Efficient Fenestration: Brief Survey and Update on Thermochromics and Electrochromics. *J. Vac. Sci. Technol., B: Nanotechnol. Microelectron.: Mater., Process., Meas., Phenom.* **2014**, *32*, 060801.

(7) Wen, R.-T.; Niklasson, G. A.; Granqvist, C. G. Electrochromic Nickel Oxide Films and Their Compatibility with Potassium Hydroxide and Lithium Perchlorate in Propylene Carbonate: Optical, Electrochemical and Stress-Related Properties. *Thin Solid Films* **2014**, *565*, 128−135.

(8) Bouessay, I.; Rougier, A.; Tarascon, J.-M. Electrochemically Inactive Nickel Oxide as Electrochromic Material. *J. Electrochem. Soc.* **2004**, *151*, H145.

(9) Kalyuzhny, G.; Vaskevich, A.; Schneeweiss, M. A.; Rubinstein, I. Transmission Surface-Plasmon Resonance (T-SPR) Measurements for Monitoring Adsorption on Ultrathin Gold Island Films. *Chemistry* **2002**, *8*, 3849−3857.

(10) Doron-Mor, I.; Barkay, Z.; Filip-Granit, N.; Vaskevich, A.; Rubinstein, I. Ultrathin Gold Island Films on Silanized Glass. Morphology and Optical Properties. *Chem. Mater.* **2004**, *16*, 3476−3483.

(11) Bonaccorso, F.; Colombo, L.; Yu, G.; Stoller, M.; Tozzini, V.; Ferrari, A. C.; Ruoff, R. S.; Pellegrini, V. Graphene, Related Two-Dimensional Crystals, and Hybrid Systems for Energy Conversion and Storage. *Science* **2015**, *347*, 1246501−1246501.

(12) Miao, X.; Tongay, S.; Petterson, M. K.; Berke, K.; Rinzler, A. G.; Appleton, B. R.; Hebard, A. F. High Efficiency Graphene Solar Cells by Chemical Doping. *Nano Lett.* **2012**, *12*, 2745−2750.

(13) Wang, J. T.-W.; Ball, J. M.; Barea, E. M.; Abate, A.; Alexander-Webber, J. A.; Huang, J.; Saliba, M.; Mora-Sero, I.; Bisquert, J.; Snaith, H. J.; Nicolas, R. J. Low-Temperature Processed Electron Collection Layers of Graphene/TiO_2 Nanocomposites in Thin Film Perovskite Solar Cells. *Nano Lett.* **2014**, *14*, 724−730.

(14) Lin, J.; Raji, A.-R. O.; Nan, K.; Peng, Z.; Yan, Z.; Samuel, E. L. G.; Natelson, D.; Tour, J. M. Iron Oxide Nanoparticle and Graphene Nanoribbon Composite as an Anode Material for High-Performance Li-Ion Batteries. *Adv. Funct. Mater.* **2014**, *24*, 2044−2048.

(15) Wang, H.; Cui, L.-F.; Yang, Y.; Sanchez Casalongue, H.; Robinson, J. T.; Liang, Y.; Cui, Y.; Dai, H. Mn_3O_4-Graphene Hybrid as a High-Capacity Anode Material for Lithium Ion Batteries. *J. Am. Chem. Soc.* **2010**, *132*, 13978−13980.

(16) Zhao, X.; Hayner, C. M.; Kung, M. C.; Kung, H. H. In-Plane Vacancy-Enabled High-Power Si-Graphene Composite Electrode for Lithium-Ion Batteries. *Adv. Energy Mater.* **2011**, *1*, 1079−1084.

(17) Cai, G.; Tu, J.; Zhang, J.; Mai, Y.; Lu, Y.; Gu, C.; Wang, X. An Efficient Route to a Porous NiO/Reduced Graphene Oxide Hybrid Film with Highly Improved Electrochromic Properties. *Nanoscale* **2012**, *4*, 5724−5730.

(18) Kholmanov, I. N.; Magnuson, C. W.; Aliev, A. E.; Li, H.; Zhang, B.; Suk, J. W.; Zhang, L. L.; Peng, E.; Mousavi, S. H.; Khanikaev, A. B.; Piner, R.; Shvets, G.; Ruoff, R. S. Improved Electrical Conductivity of Graphene Films Integrated with Metal Nanowires. *Nano Lett.* **2012**, *12*, 5679−5683.

(19) Palenzuela, J.; Viñuales, A.; Odriozola, I.; Cabañero, G.; Grande, H. J.; Ruiz, V. Flexible Viologen Electrochromic Devices with Low Operational Voltages Using Reduced Graphene Oxide Electrodes. *ACS Appl. Mater. Interfaces* **2014**, *6*, 14562−14567.

(20) Bao, W.; Wan, J.; Han, X.; Cai, X.; Zhu, H.; Kim, D.; Ma, D.; Xu, Y.; Munday, J. N.; Drew, H. D.; Fuhrer, M. S.; Hu, L. Approaching the Limits of Transparency and Conductivity in Graphitic Materials Through Lithium Intercalation. *Nat. Commun.* **2014**, *5*, 4224.

(21) Polat, E. O.; Balci, O.; Kocabas, C. Graphene Based Flexible Electrochromic Devices. *Sci. Rep.* **2014**, *4*, 6484.

(22) Bult, J. B.; Crisp, R.; Perkins, C. L.; Blackburn, J. L. Role of Dopants in Long-Range Charge Carrier Transport for P-Type and N-Type Graphene Transparent Conducting Thin Films. *ACS Nano* **2013**, *7*, 7251−7261.

(23) Li, X.; Cai, W.; An, J.; Kim, S.; Nah, J.; Yang, D.; Piner, R.; Velamakanni, A.; Jung, I.; Tutuc, E.; Banerjee, S. K.; Colombo, L.; Ruoff, R. S. Large-Area Synthesis of High-Quality and Uniform Graphene Films on Copper Foils. *Science* **2009**, *324*, 1312−1314.

(24) Bae, S.; Kim, H.; Lee, Y.; Xu, X.; Park, J.-S.; Zheng, Y.; Balakrishnan, J.; Lei, T.; Kim, H. R.; Song, Y.; Kim, Y.-J.; Kim, K. S.; Ozyilmaz, B.; Ahn, J.-H.; Hong, B. H.; Iijima, S. Roll-to-Roll Production of 30-Inch Graphene Films for Transparent Electrodes. *Nat. Nanotechnol.* **2010**, *5*, 574−578.

(25) Lin, F.; Nordlund, D.; Weng, T.-C.; Sokaras, D.; Jones, K. M.; Reed, R. B.; Gillaspie, D. T.; Weir, D. G. J.; Moore, R. G.; Dillon, A. C.; Richards, R. M.; Engtrakul, C. Origin of Electrochromism in High-Performing Nanocomposite Nickel Oxide. *ACS Appl. Mater. Interfaces* **2013**, *5*, 3643−3649.

(26) Lin, F.; Nordlund, D.; Weng, T.-C.; Moore, R. G.; Gillaspie, D. T.; Dillon, A. C.; Richards, R. M.; Engtrakul, C. Hole Doping in Al-Containing Nickel Oxide Materials to Improve Electrochromic Performance. *ACS Appl. Mater. Interfaces* **2013**, *5*, 301−309.

(27) Lin, F.; Montano, M.; Tian, C.; Ji, Y.; Nordlund, D.; Weng, T.-C.; Moore, R. G.; Gillaspie, D. T.; Jones, K. M.; Dillon, A. C.; Richards, R. M.; Engtrakul, C. Electrochromic Performance of

Nanocomposite Nickel Oxide Counter Electrodes Containing Lithium and Zirconium. *Sol. Energy Mater. Sol. Cells* **2014**, *126*, 206−212.
(28) Malard, L. M.; Pimenta, M. A.; Dresselhaus, G.; Dresselhaus, M. S. Raman Spectroscopy in Graphene. *Phys. Rep.* **2009**, *473*, 51−87.
(29) Ferrari, A. C. Raman Spectroscopy of Graphene and Graphite: Disorder, Electron−Phonon Coupling, Doping, and Nonadiabatic Effects. *Solid State Commun.* **2007**, *143*, 47−57.
(30) Cançado, L. G.; Jorio, A.; Ferreira, E. H. M.; Stavale, F.; Achete, C. A.; Capaz, R. B.; Moutinho, M. V. O.; Lombardo, A.; Kulmala, T. S.; Ferrari, A. C. Quantifying Defects in Graphene via Raman Spectroscopy at Different Excitation Energies. *Nano Lett.* **2011**, *11*, 3190−3196.
(31) Das, A.; Chakraborty, B.; Sood, A. K. Raman Spectroscopy of Graphene on Different Substrates and Influence of Defects. *Bull. Mater. Sci.* **2008**, *31*, 579−584.
(32) Li, X.; Zhu, Y.; Cai, W.; Borysiak, M.; Han, B.; Chen, D.; Piner, R. D.; Colombo, L.; Ruoff, R. S. Transfer of Large-Area Graphene Films for High-Performance Transparent Conductive Electrodes. *Nano Lett.* **2009**, *9*, 4359−4363.
(33) Primak, W.; Fuchs, L. H. Electrical Conductivities of Natural Graphite Crystals. *Phys. Rev.* **1954**, *95*, 22.
(34) Wallace, P. R. The Band Theory of Graphite. *Phys. Rev.* **1947**, *71*, 622.
(35) Armstrong, N. R.; Veneman, P. A.; Ratcliff, E.; Placencia, D.; Brumbach, M. Oxide Contacts in Organic Photovoltaics: Characterization and Control of Near-Surface Compoisition in Indium-Tin Oxide (ITO) Electrodes. *Acc. Chem. Res.* **2009**, *42*, 1748−1757.

DOI: 10.1021/acsami.5b01777
ACS Appl. Mater. Interfaces 2015, 7, 11330−11336